

Article

High-Resolution Radio Observations of Five Optically Selected Type 2 Quasars

Máté Krezinger ^{1,2}, Sándor Frey ^{2,3}, Zsolt Paragi ⁴ and Roger Deane ^{5,6,*}¹ Department of Astronomy, Eötvös Loránd University, Pázmány Péter sétány 1/A, H-1117 Budapest, Hungary² Konkoly Observatory, Research Centre for Astronomy and Earth Sciences, Konkoly Thege Miklós út 15-17, H-1121 Budapest, Hungary; frey.sandor@csfk.mta.hu³ Institute of Physics, ELTE Eötvös Loránd University, Pázmány Péter sétány 1/A, H-1117 Budapest, Hungary⁴ Joint Institute for VLBI ERIC, Oude Hoogeveensedijk 4, 7991 PD, Dwingeloo, The Netherlands; zparagi@jive.eu⁵ Department of Physics, University of Pretoria, Hatfield, Pretoria 0028, South Africa; roger.deane@up.ac.za⁶ Centre for Radio Astronomy Techniques and Technologies, Department of Physics and Electronics, Rhodes University, Mkhanda 6140, South Africa

* Correspondence: krezinger.mate@csfk.mta.hu

Received: 27 February 2020; Accepted: 30 March 2020; Published: date



Abstract: Many low-luminosity active galactic nuclei (AGNs) contain a compact radio core which can be observed with high angular resolution using very long baseline interferometry (VLBI). Combining arcsec-scale structural information with milliarcsec-resolution VLBI imaging is a useful way to characterise the objects and to find compact cores on parsec scales. VLBI imaging could also be employed to look for dual AGNs when the sources show kpc-scale double symmetric structure with flat or inverted radio spectra. We observed five such sources at redshifts $0.36 < z < 0.58$ taken from an optically selected sample of Type 2 quasars with the European VLBI Network (EVN) at 1.7 and 5 GHz. Out of the five sources, only one (SDSS J1026–0042) shows a confidently detected compact VLBI core at both frequencies. The other four sources are marginally detected at 1.7 GHz only, indicating resolved-out radio structure and steep spectra. Using first-epoch data from the ongoing Karl G. Jansky Very Large Array Sky Survey, we confirm that indeed all four of these sources have steep radio spectra on arcsec scale, contrary to the inverted spectra reported earlier in the literature. However, the VLBI-detected source, SDSS J1026–0042, has a flat integrated spectrum. Radio AGNs that show kpc-scale symmetric structures with truly flat or inverted spectra could still be promising candidates of dual AGNs, to be targeted with VLBI observations in the future.

Keywords: active galactic nuclei; quasars; radio continuum; radio spectrum; interferometry; imaging

1. Introduction

Despite decades of detailed investigation, the true nature of the low-luminosity active galactic nuclei (LLAGNs, e.g., Seyferts and LINERs) is still under debate. More than 40% of galaxies in the local Universe contain LLAGN [1]. Since they are much fainter (with bolometric luminosity $L_{\text{bol}} < 10^{38}$ W and radio power $P_{1.4\text{GHz}} < 10^{35}$ W Hz⁻¹) than the radio-loud AGNs and typically lack prominent, extended jets, it is more difficult to observe them. As with all AGNs, these sources are also powered by accretion onto a supermassive black hole, but with a lower accretion rate. Thus they appear as “downscaled” AGNs (e.g., [2]). These sources show mostly low ionization state optical emission lines in their spectra [1], and have

low accretion rates ($< 10^{-2} - 10^{-3}$ times the Eddington rate [3]). LLAGNs also have radio emission that seems originating from compact jets on parsec (pc) scales [3–5].

Using the technique of very long baseline interferometry (VLBI), we can directly observe compact pc or even sub-pc scale radio emission. The baselines of the globally distributed radio telescope arrays, such as the European VLBI Network (EVN), are up to a few thousand kilometers long, providing milliarcsec (mas) or sub-mas resolution, depending on the observing frequency. Because of the high resolution, a VLBI detection of a radio source at GHz frequencies typically implies high brightness temperatures ($T_b > 10^{6-7}$ K) that can be produced by the non-thermal (synchrotron) emission of AGNs [6,7]. A radio power exceeding 10^{21} W Hz $^{-1}$ in a source unresolved by the Karl G. Jansky Very Large Array (VLA) on arcsec scales is already indicative of accretion-powered nuclear activity [7] or maybe circumnuclear starburst. Detection of a compact core with VLBI in a high-luminosity source is a very strong AGN indicator.

In LLAGNs, compact radio emission with flat (i.e., with spectral index $-0.5 \leq \alpha \leq 0$, where the flux density is $S \propto \nu^\alpha$, and ν is the frequency) or inverted ($\alpha > 0$) radio continuum spectrum can indicate radio emission that is fueled by a synchrotron self-absorbed jet base coupled to an underluminous accretion disk (e.g., [4]) or an accretion inflow onto the black hole [8]. When observed at high frequencies, magnetized plasma in the accretion disc corona can also produce compact sub-pc scale optically thick flat-spectrum radio emission ([9] and references therein). On the other hand, external free-free absorption of non-thermal radio emission can cause flat spectrum by flattening the steep-spectrum ($\alpha < -0.5$) external emission [10,11], although it would have brightness temperature $T_b \sim 10^4$ K [12]. There is a phenomenon analogous to coronal mass ejections in active stars that could also occur in AGNs, in the form of outflowing blobs of highly magnetized plasma [13]. However, similar to jet activity, it produces extended optically thin emission with steep radio spectrum. At highly subluminal speeds, the magnetized corona could be considered as the base for jet launching ([9] and references therein).

The combination of radio interferometric measurements with the VLA and VLBI is an effective tool to identify compact cores in LLAGNs (see [3,5] and references therein). At GHz frequencies, obscuration effects are minimal compared to the infrared or ultra-violet regimes, and sensitive high-resolution radio maps of a source can be produced with typically less than 1–2 h of observation. The arcsec-scale multi-frequency VLA imaging can provide essential spectral and structural information [14,15], which can help selecting targets for follow-up VLBI observations of the mas-scale radio structure. With this much finer angular resolution, the extended radio emission from the host galaxy is resolved out in general, thus only the compact emission from the AGN remains to be detected. AGN cores typically have flat radio spectra, as opposed to extended jet or hot spot features. Therefore, arcsec-scale radio imaging is a useful tool to identify candidate multiple AGN systems. Sources with multiple flat-spectrum features can then be targeted with VLBI observations that provide mas-scale resolution. A compact, high brightness temperature ($T_b > 10^6$ K) component that can only be revealed with VLBI is a clear indication of AGN core emission ([16,17] and references therein).

This method could offer an excellent means for finding multiple AGNs with kpc separation. Dual AGNs are expected at stages of galaxy evolution driven by mergers throughout the history of the Universe. While their observational identification is challenging, their study is important in many areas of current cosmology and multi-messenger astrophysics (see [16,17] and references therein). VLBI observations of a large sample of arcsec-scale double radio AGNs with flat/inverted overall spectra would provide an opportunity to estimate the prevalence of dual radio-emitting AGNs in an unbiased way. Synchrotron self-absorbed jets, and emission from a magnetically-heated corona in an accretion disc can show flat/inverted spectrum [18,19]. In either case, the compact double structure would indicate dual AGN activity since the detection of mas-scale emission at GHz frequencies is directly related to AGN activity in sources above redshift $z \approx 0.1$ [17]. As compact cores are relatively common in LLAGNs, they are good candidates for finding dual AGNs. This would provide an efficient selection method that can

be applied for future sub-arcsec resolution interferometer surveys, such as the ones using the SKA [20]. Securely confirming dual AGN candidates is not a trivial task that can solely rely on radio measurements. It often benefits from observations at multiple wavebands, from optical to X-rays, using both spatially resolved spectroscopic and imaging techniques [17,21].

In this paper, we report on the observations of five LLAGNs with the EVN at two frequencies, 1.7 and 5 GHz. Section 2 presents the sample and its selection. Section 3 gives details about the radio interferometric observations. The data analysis and the result are described in Section 4, and our findings are discussed in Section 5. We conclude the paper in Section 6. Throughout this study, we adopt a standard flat Λ Cold Dark Matter cosmology with $\Omega_m = 0.3$, $\Omega_\Lambda = 0.7$, and $H_0 = 70 \text{ km s}^{-1} \text{ Mpc}^{-1}$ for calculating luminosities and projected linear sizes [22].

2. Sample Selection and Observing Goals

We selected five sources for mas-resolution follow-up VLBI observations from the sample of [11]. Our target sources are listed in Table 1. These were previously observed in the radio at 8.4 GHz with the VLA in its B configuration [11], providing typical angular resolution of about 1 arcsec or somewhat below. Originally, the sources were taken from the optically selected sample of Zakamska et al. [23], which was the first comprehensive survey for studying the optical properties of Type 2 quasars (i.e., quasars where the accretion disk is seen nearly “edge-on”, and the disk and the broad-line region are obscured by the surrounding torus of dense gas and dust) in detail using SDSS data. Each of the five sources we selected (Table 1) showed symmetric double radio structure on arcsec angular scales in the 8.4-GHz VLA images, and their overall radio spectra were reported to be inverted [11]. Two of our targets, J0741+3020 and J0956+5735, were included in the sample of Bellocchi et al. [24], who looked for ionized gas outflows in obscured quasars. According to their optical spectroscopic observations, outflows are detected in both objects. J0741+3020 is associated with a giant ($> 100 \text{ kpc}$) ionized nebula, while in the case of J0956+5735, the compact [OIII] profile suggests a spatially unresolved outflow [24]. The host galaxies of three of these AGNs are morphologically classified from SDSS or *Hubble Space Telescope* images as bulge-dominated elliptical/S0 galaxies (Table 1), with J0741+3020 as an ULIRG elliptical in a multiple system [24,25]. J1447+0211 is difficult to classify as it appears highly disturbed due to a recent galaxy interaction [26]. It shows optical features such as tidal tails, bridge, and even double nuclei with 1.5 kpc separation. For the host galaxy of J1026–0042, no classification is found in the literature.

Table 1. Name, J2000 optical equatorial coordinates, redshift, VLA 8.4-GHz radio flux density, 1.4–8.4 GHz spectral index, and optical magnitude of the five sources selected from Lal & Ho [11]. The coordinates are taken from the SDSS Data Release 15 [27] and, for SDSS J1026–0042, the *Gaia* Data Release 2 [28,29]. The SDSS *r*-band magnitudes are adopted from Zakamska et al. [23]. The morphological types of the visually classified host galaxies are obtained from the works in [24–26]. HD means highly disturbed from galaxy interaction.

ID	Right Ascension			Declination			z	$S_{8.4\text{GHz}}$ mJy	$\alpha_{1.4}^{8.4}$	<i>r</i> mag	Host Galaxy
	h	min	s	°	'	''					
SDSS J0741+3020	07	41	30.513	+30	20	05.186	0.476	2.97	+0.56	21.06	ULIRG
SDSS J0956+5735	09	56	29.058	+57	35	08.775	0.361	2.88	+0.72	20.18	E/S0
SDSS J1014+0244	10	14	03.524	+02	44	16.521	0.573	4.53	+0.45	21.51	E/S0
SDSS J1026–0042	10	26	40.437	–00	42	06.484	0.364	3.68	+0.38	19.73	...
SDSS J1447+0211	14	47	11.292	+02	11	36.234	0.386	2.76	+0.85	20.35	HD

Our sources selected for VLBI observations (Table 1) fall in the radio-intermediate regime, between the radio-quiet and radio-loud AGNs. Interestingly, most of the sources in the 8.4-GHz VLA sample [11] with flat or inverted spectra are radio-intermediate objects, and some of them show extended symmetric double structure on arcsec scale. A flat/inverted spectrum may indicate free–free absorption by ionized gas in

the narrow-line region. This finding was rather unusual, which prompted us to probe the structure of our sub-sample of “best established” symmetric sources (Table 1) on mas scales with VLBI observations. Finding a mas-scale compact radio core with deep VLBI imaging could in principle pin down the location of the AGN, which has been found offset from the optical position in a number of cases (e.g., [8]), while the extended radio emission should be completely resolved out (undetected) on the long interferometer baselines. Although an unlikely scenario for the given sample, one could even find instead two compact VLBI cores corresponding to dual AGN activity, given the symmetric flat/inverted components seen on VLA scales. In this case, the arcsec-scale symmetric double radio structure could be explained by simultaneous activity in both AGNs.

3. Observational Data

3.1. EVN observations

We observed the five selected targets (Table 1) with the EVN at 1.7 and 5 GHz, to attempt the detection of mas-scale compact radio components in these LLAGNs. The observations were carried out on 5 June 2015 (5 GHz) and 15 June 2015 (1.7 GHz) under the project code EP093. The total bandwidth of 128 MHz was divided into eight intermediate frequency channels (IFs) containing thirty-two 500-kHz wide spectral channels each, in both left and right circular polarizations. The following 13 radio observatories participated in the experiments: Jodrell Bank Mk2 25-m (Great Britain), Westerbork 25-m (The Netherlands), Effelsberg 100-m (Germany), Medicina 32-m, Noto 32-m (Italy), Onsala 25-m (Sweden), Sheshan 25-m (China), Toruń 32-m (Poland), Yebes 40-m (Spain), Svetloe 32-m, Zelenchuckskaya 32-m, Badary 32-m (Russia), and Hartebeesthoek 26-m (South Africa). The data were recorded at 1024 Mbits^{-1} rate and correlated at JIVE. We applied the technique of phase referencing [30] and subsequently pointed the radio telescopes to a nearby bright compact calibrator source and the given target, in a repeated 5-min cycle. Within each cycle, ~ 3.5 min was spent on the weak target source. The delay, rate, and phase solutions derived for the phase-reference calibrators (J0741+3112, J0956+5753, J1015+0109, J1024–0052, and J1440+0157) could later be interpolated and applied to the corresponding target source data, to allow for longer coherent integration and thus an improved sensitivity for the weaker LLAGNs. The calibrator–target separations were 0.87° , 0.31° , 1.65° , 0.57° , and 1.57° , respectively. The total on-source integration time for each target was ~ 80 min.

3.2. VLA Sky Survey Data

We obtained the raw 8.4-GHz VLA data analyzed by Lal & Ho [11] from the NRAO Archive (<http://archive.nrao.edu/>) (project code AV288) and calibrated them in a standard way using the NRAO AIPS software (<http://www.aips.nrao.edu/index.shtml>), but failed to reproduce the images of our five target sources. To obtain independent information on the overall radio spectrum of the sources, we then turned to the publicly available preliminary radio images from the ongoing VLASS [15] at 2.7 GHz and compared the obtained flux densities to the 1.4-GHz values in the FIRST survey catalogue [31]. The VLASS supersedes previous VLA radio sky surveys at GHz frequencies such as the NVSS [32] in terms of angular resolution and sensitivity. In 2019, the first phase of the survey was completed with covering the entire sky north of -40° declination at the 2–4 GHz frequency range in total intensity (Stokes I). The angular resolution is $2.5''$ and the imaging sensitivity is $\sigma \sim 120 \mu\text{Jy beam}^{-1}$ at the first survey epoch. Later, with the planned three epochs combined, the sensitivity should reach $\sim 70 \mu\text{Jy beam}^{-1}$. All our target sources fall into the VLASS coverage area. Quick Look images with $1^\circ \times 1^\circ$ field size are available in the VLASS archive (<https://archive-new.nrao.edu/vlass/>). Five tiles (T18t11, T25t08, T11t16, T10t16, and T11t23) were selected based on the celestial coordinates, corresponding to our targets in the order of their appearance in Table 1. The Quick Look images are capable of revealing

arcsec-scale morphological features of radio galaxies like radio cores and jets [33]; however, they may suffer from deconvolution issues due to the extremely short integrations and resultant (u, v) coverage.

4. Data Analysis and Results

4.1. EVN Data

The raw correlated VLBI visibility data that are now in public domain and can be obtained from the EVN Data Archive (https://old.jive.nl/archive-info?experiment=EP093A_150605 and https://old.jive.nl/archive-info?experiment=EP093B_150615) were loaded into AIPS for initial calibration. We followed standard procedures [34]. At the beginning, the data affected by known problems with antenna pointing and radio frequency interference were flagged. The visibility amplitudes were calibrated using antenna gains and system temperatures measured at the telescope sites. We used nominal system temperature values where measurements were unavailable. We corrected for the dispersive ionospheric delay using total electron content maps derived from global navigation satellite systems data, and also applied parallactic angle corrections. Using a 1-min scan on the strong fringe-finder source 0528+134, we performed an initial correction of instrumental phases and delays. We then performed fringe-fitting for all the five phase-reference calibrator sources and the fringe-finders (0528+134, 3C 138, and 4C 39.25) scheduled in the experiments. These calibrated visibility data were exported to the Difmap package [35] for hybrid mapping. This involved iterations of the CLEAN algorithm and phase-only self calibration, and finally phase and amplitude self-calibration. We used the brightness distribution models obtained for the calibrator and fringe-finder sources to derive overall antenna gain correction factors (up to 6% in case of some antennas). These were applied in AIPS to the target source data as well, to refine the initial amplitude calibration. As the next step, we repeated fringe-fitting for the five phase-reference calibrators in AIPS. This time the CLEAN component models of their brightness distributions were used as an input, to account for any residual phases due to their mas-scale structure. The solutions were interpolated and applied to the data of the respective target sources.

The calibrated and phase-referenced visibility data of the targets (J0741+3020, J0956+5735, J1014+0244, J1026–0042, and J1447+0211) were transferred from AIPS to Difmap for imaging. We applied natural weighting with the visibility errors raised to the power -1 (`uvweight 0, -1` command in Difmap) in order to minimize the image noise. At both observing frequencies, 1.7 and 5 GHz, the dirty images of all target sources but J1026–0042 showed peaks with signal-to-noise ratios below 7, as seen in a rectangular field of view of $512 \text{ mas} \times 512 \text{ mas}$ centered on the brightest pixel. Therefore, we regard J0741+3020, J0956+5735, J1014+0244, and J1447+0211 as non-detections with the EVN. For J1026–0042, the calibrated visibility data were fitted directly with a circular Gaussian brightness distribution model in Difmap [35]. The images of J1026–0042 at both frequencies are displayed in Figure 1.

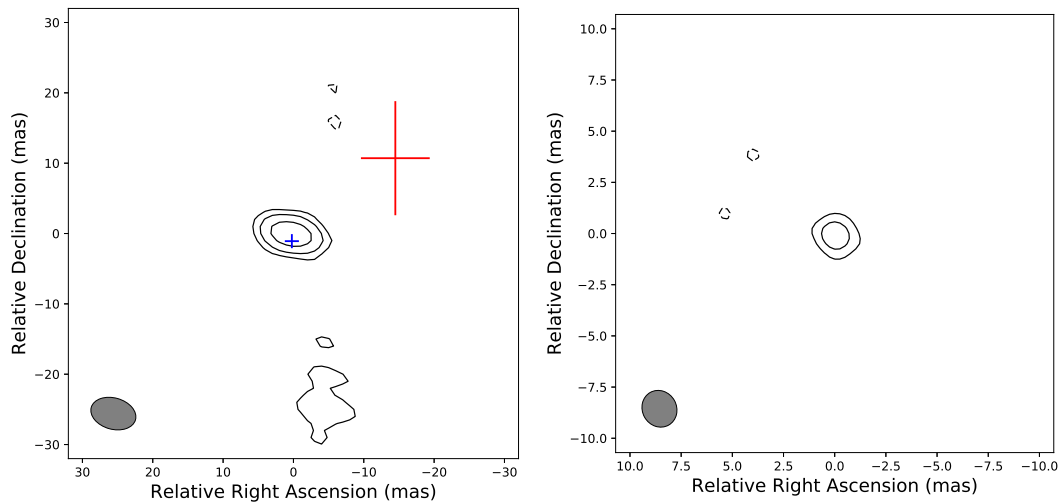


Figure 1. VLBI images of SDSS J1026–0042 at 1.7 GHz (left) and 5 GHz (right). The red cross marks the *Gaia* DR2 optical position [28,29], the blue cross indicates the EVN 5 GHz position (see Section 5.1). The peak brightness values are $1.01 \text{ mJy beam}^{-1}$ at 1.7 GHz, and $0.20 \text{ mJy beam}^{-1}$ at 5 GHz. The contour levels are drawn at $3\sigma \times (-1, 1, 2, 4)$, where the 3σ image noise is $165 \mu\text{Jy beam}^{-1}$ and $65 \mu\text{Jy beam}^{-1}$ at 1.7 and 5 GHz, respectively. The size of the elliptical Gaussian restoring beam (HPBW) is shown as an ellipse in the lower-left corner of the images. The HPBW is $6.5 \text{ mas} \times 4.5 \text{ mas}$ with a major axis position angle $PA = 74.3^\circ$ (measured from north through east) at 1.7 GHz, and $1.83 \text{ mas} \times 1.67 \text{ mas}$ with $PA = 29.2^\circ$ at 5 GHz.

At 1.7 GHz, looking at the EVN dirty images of a larger ($4.096'' \times 4.096''$) field of view, the remaining four sources (J0741+3020, J0956+5735, J1014+0244, and J1447+0211) have an SNR slightly above 7. Here, we also used natural weighting with the visibility errors raised to the power -1 , except for J0741+3020 and J1447+0211, where the power of -2 was applied in Difmap. Therefore, these LLAGNs are marginally detected with the EVN at 1.7 GHz only, but the strong side lobe patterns in the dirty images prevent us from locating the source with high confidence, and brightness distribution models cannot be reliably fitted to the visibility data of these weak VLBI sources. This is typical for extended sources when only the shortest interferometer baselines detect the emission. We tentatively assume that the brightness peak of the dirty image coincides with the AGN core.

4.2. VLA Data

To determine the VLASS flux densities, we loaded the Quick Look images covering our target sources into AIPS. We used the task JMFIT to fit a circular Gaussian to the image data at the given positions (see Table 1). The typical brightness uncertainty of the VLASS images is $\approx 15\%$ [36]. We adopted this as the error of the fitted 2.7-GHz flux density values that are given in Table 2, along with the fitted 1.7- and 5-GHz EVN flux densities in the case of J1026–0042. For the remaining four LLAGNs considered to be marginally detected at 1.7 GHz and not detected at 5 GHz with the EVN, at the latter frequency, we give flux density upper limits for any compact radio source of the restoring beam size of about $1.5 \text{ mas} \times 2.5 \text{ mas}$, based on the 7σ image noise level. At 1.7 GHz, we can obtain a flux density estimate of the radio emission that is mostly resolved out by the EVN, by means of fitting a circular Gaussian model at the brightness peak location in the extended-field dirty maps. These models should be treated with caution and considered as tentative only. However, as we show below, the flux density values determined this way are consistent with the VLA data measured at close-by frequencies.

Table 2. Flux densities with their associated uncertainties and the derived $\alpha_{1.4}^{2.7}$ spectral indices of the target sources.

ID	$S_{1.4\text{ GHz}}$ mJy	$S_{1.7\text{ GHz}}$ mJy	$S_{2.7\text{ GHz}}$ mJy	$S_{5\text{ GHz}}$ mJy	$S_{8.4\text{ GHz}}$ mJy	$\alpha_{1.4}^{2.7}$
SDSS J0741+3020	1.12 ± 0.16	0.28 ± 0.03	0.79 ± 0.12	<0.08	2.97 ± 0.01	-0.53 ± 0.04
SDSS J0956+5735	0.88 ± 0.15	0.71 ± 0.07	0.47 ± 0.07	<0.08	2.88 ± 0.01	-0.95 ± 0.03
SDSS J1014+0244	2.02 ± 0.13	1.70 ± 0.17	1.20 ± 0.18	<0.11	4.53 ± 0.02	-0.80 ± 0.07
SDSS J1026–0042	1.85 ± 0.15	1.24 ± 0.12	1.63 ± 0.24	0.20 ± 0.02	3.68 ± 0.02	-0.20 ± 0.09
SDSS J1447+0211	0.76 ± 0.15	0.23 ± 0.02	0.55 ± 0.08	<0.08	2.76 ± 0.01	-0.49 ± 0.08

Notes: Column 2, VLA [11,31]; Column 3, EVN (this paper); Column 4, VLA [15]; Column 5, EVN (this paper); Column 6, VLA [11]; Column 7, two-point spectral index calculated from the arcsec-scale VLA (1.4-GHz FIRST and 2.7-GHz VLASS) measurements [15,31]

5. Discussion

5.1. VLBI Structure of the Target Sources

From the five targeted LLAGN sources, only SDSS J1026–0042 was firmly detected with the EVN. One source component was found at both observing frequencies, 1.7 and 5 GHz. The VLBI positions (the coordinates corresponding to the origin of the maps in Figure 1) agree with each other within the uncertainty of about 1 mas. At both frequencies, the component is seen as a compact source. We calculated the minimum resolvable angular size with the interferometer using Equation (2) of [37]. The single detected component in SDSS J1026–0042 is resolved at both frequencies as the fitted circular Gaussian diameters, 0.79 ± 0.06 mas and 0.065 ± 0.007 mas (FWHM) at 1.7 and 5 GHz, respectively, are larger than the minimum resolvable sizes. The size uncertainties were calculated following Fomalont [38]. Using the AIPS task MAXFIT, the peak position of the 5-GHz image is at right ascension $\alpha_{\text{EVN}} = 10^{\text{h}}26^{\text{m}}40.4381^{\text{s}}$ and declination $\delta_{\text{EVN}} = -00^{\circ}42'06.496''$. In comparison, the most accurate optical position taken from the *Gaia* Data Release 2 [28,29] database (<https://gea.esac.esa.int/archive/>) is $\alpha_{\text{Gaia}} = 10^{\text{h}}26^{\text{m}}40.4371^{\text{s}} \pm 0.0003^{\text{s}}$, $\delta_{\text{Gaia}} = -00^{\circ}42'06.4843'' \pm 0.0081''$. There is a radio–optical positional difference of ~ 15 mas in right ascension and ~ 10 mas in declination (Figure 1). Given that the EVN positions are accurate to within 1 mas, and for the optical position the uncertainties are $\Delta\alpha \approx 5$ mas and $\Delta\delta \approx 8$ mas, the difference is significant. At $z = 0.364$, this corresponds to $(\sim 90 \pm 40)$ pc projected linear distance between the *Gaia* optical and the VLBI radio position. According to Plavin et al. [39], at least 20–50 pc projected difference between the VLBI and *Gaia* positions is quite common in bright AGNs. They also found that in 80% of Seyfert 2 galaxies, the associated *Gaia* position related to the jet is located farther away from the nucleus than the VLBI core. This offset could be explained by the presence of a bright extended optical jet which shifts the *Gaia* centroid [40,41]. While this interpretation might seem appealing in view of the extended lobe structure reported by Lal & Ho [11], in our VLBI data, we do not find any supporting evidence for large scale-jets, which makes this interpretation less likely.

Based on our EVN measurements, we derived the observed brightness temperatures of SDSS J1026–0042 at both frequencies using Equation (1) [42]. Here, z is the redshift, S_{ν} is the flux density (measured in Jy) at ν frequency (GHz), and θ is the FWHM of the fitted circular Gaussian model component (mas).

$$T_{\text{b,obs}} = 1.22 \times 10^{12} (1+z) \frac{S_{\nu}}{\theta^2 \nu^2} \quad [\text{K}] \quad (1)$$

The derived values are $T_{\text{b,obs}} = (1.15 \pm 0.22) \times 10^9$ K at 1.7 GHz, and $T_{\text{b,obs}} = (3.01 \pm 0.74) \times 10^9$ K at 5 GHz. The values $T_{\text{b,obs}} > 10^6$ K indicate non-thermal emission originating from AGN (e.g., [7]). We also derived the K -corrected monochromatic radio power values for the compact VLBI-detected components of SDSS J1026–0042: $P_{1.7\text{ GHz}} = (7.08 \pm 0.48) \times 10^{23}$ W Hz $^{-1}$ and $P_{5\text{ GHz}} = (1.10 \pm 0.13) \times 10^{23}$ W Hz $^{-1}$. For this

calculation, we used Equation (2), where D_L is the luminosity distance and $\alpha = -1.73$ is the spectral index between 1.7 and 5 GHz derived from our VLBI model component flux densities (Table 2).

$$P_\nu = 4\pi D_L^2 S_\nu (1+z)^{-1-\alpha} \quad (2)$$

With these values at hand, we can assess whether the radio emission could originate from supernova remnants in the host galaxy [7]. The supernova rate corresponding to our radio powers ($\nu_{SN} = 149$ and 52 yr^{-1} at 1.7 and 5 GHz, respectively) exceeds the rates of the most powerful starburst galaxies (e.g., [43,44]). An individual supernova remnant is also ruled out, and complexes of supernova remnants do not concentrate at mas scales. A recent study investigating radio-quiet AGNs at $z < 0.8$, with $4 \times 10^{21} < P_{1.4\text{GHz}} < 7 \times 10^{24} \text{ W Hz}^{-1}$, and $L_{\text{bol}} < 10^{38} \text{ W}$ [45] concluded that the radio emission originating from these sources is dominated by AGN activity and not the host galaxy. Similar results were found by Herrera Ruiz et al. [6] and Maini et al. [46].

5.2. The Marginally Detected Sources

As mentioned in Section 4, we marginally detected four target sources in the 1.7-GHz EVN dirty images. This suggests the presence of some extended radio emission that is, however, completely resolved out on the long baselines. On the other hand, these sources remained undetected at 5 GHz.

We tentatively locate them at the respective brightness peaks of the phase-referenced EVN dirty maps. These coordinates are given in Table 3, along with a radio–optical angular separation based on the optical coordinates in SDSS DR15 [27,47] (see Table 1). Unfortunately, unlike for SDSS J1026–0042, there are no accurate *Gaia* optical positions available for these LLAGNs. The SDSS positions are known to be accurate to $\sim 60 \text{ mas}$ (1σ) in both right ascension and declination [48], but Skipper & Browne [49] found an excess of nearby ($z < 0.2$) extragalactic sources with SDSS–radio positional separations larger than $\sim 150 \text{ mas}$, which may be caused by various effects. Therefore, our tentative radio positions seem to be consistent with the optical ones within the rather large uncertainties. More sensitive VLBI observations, possibly involving baselines providing intermediate ($\sim 100\text{-mas}$) angular resolution would be needed for reliable detection and imaging of these four sources, and for determining their accurate radio positions.

Table 3. Tentative VLBI positions of the sources marginally detected with the EVN at 1.7 GHz, and the radio–optical positional offsets.

ID	Right Ascension			Declination			$\Delta_{\text{radio-opt}}$ mas
	h	min	s	°	'	''	
SDSS J0741+3020	07	41	30.518	+30	20	05.245	98
SDSS J0956+5735	09	56	29.046	+57	35	08.751	186
SDSS J1014+0244	10	14	03.513	+02	44	16.265	310
SDSS J1447+0211	14	47	11.283	+02	11	36.389	203

5.3. Our Target Sources in the VLASS

The VLASS data that became available recently [15] allowed us to estimate the radio spectral indices of the target sources, independently of Lal & Ho [11]. Four of the five sources have been clearly detected with the VLASS at the first epoch (Table 2). In the case of SDSS J0956+5735, there appears a $\sim 4 \sigma$ peak coinciding with the optical position, suggesting the presence of a radio source. In the future, in the completed VLASS with three epochs combined, this source should also become securely detected. Apart from the poorer sensitivity, the angular resolution of the 2.7-GHz VLASS images is about three times lower than that of the 8.4-GHz VLA images presented by Lal & Ho [11], making the direct comparison of the arcsec-scale source structures difficult.

Nonetheless, the VLASS images indicate single components and not symmetric double structures, which they might not be able to resolve.

5.4. Revised Radio Spectral Indices

Based on the newly-obtained flux density data, we reexamined the radio continuum spectral properties of the target LLAGN sources. Figure 2 shows their radio spectra between 1.4 and 8.4 GHz. For recalculating the spectral indices, we used the FIRST 1.4-GHz [31] and the VLASS 2.7-GHz flux densities (Table 2), both based on VLA measurements. The resulting $\alpha_{1.4}^{2.7}$ values are given in Table 2 and Figure 2. We excluded from the spectral fit the 8.4-GHz VLA values reported by Lal & Ho [11] since those appear in most cases an order of magnitude higher than expected from the trend based on lower-frequency data. We did not include the VLBI flux density values either, because the EVN provides about three orders of magnitude higher resolution than the VLA, thus probing radio emission on a much smaller spatial scale, detecting mas-scale compact emission only. Moreover, four out of five sources are undetected at 5 GHz with the EVN, leading to flux density upper limit estimates only.

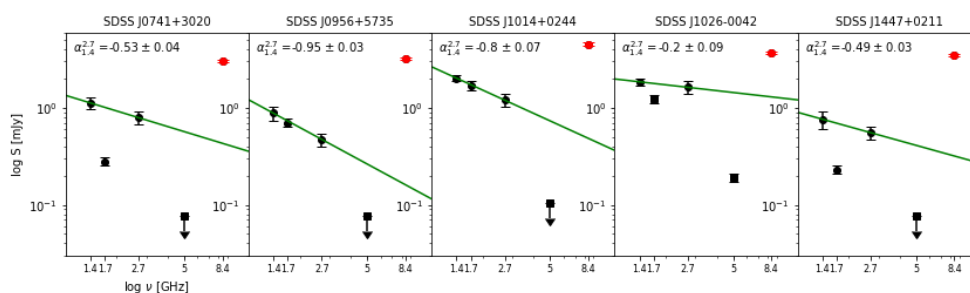


Figure 2. The continuum radio spectra of the sources between 1.4 and 5 GHz with flux density values and their associated uncertainties taken from Table 2 (black dots). For sources undetected with the EVN, flux density values at 5 GHz are shown as upper limits indicated by arrows. For SDSS J1026–0042 detected with the EVN, among the other 1.7 GHz VLBI flux densities, the values should in fact be considered as lower limits since any extended emission is resolved out on the long baselines. The green lines represent power-law spectra calculated from two VLA data points, FIRST at 1.4 GHz and VLASS at 2.7-GHz. The corresponding $\alpha_{1.4}^{2.7}$ spectral index values are displayed in the top left corner of the panels. For comparison, the 8.4-GHz VLA flux densities taken from Lal & Ho [11] are also indicated with red symbols. In all cases, these are much higher than expected from the extrapolation of 1.4- and 2.7-GHz VLA values, indicating an issue with the values derived in [11].

Considering our $\alpha_{1.4}^{2.7}$ spectral index values derived from VLA data (Table 2), the only source that has a flat radio spectrum is SDSS J1026–0042 ($\alpha_{1.4}^{2.7} = -0.20$). All others can be classified as steep-spectrum sources with spectral index below ≈ -0.5 . Notably, this finding is perfectly consistent with the fact that the only flat-spectrum source, SDSS J1026–0042, shows a compact VLBI component, while the steep-spectrum ones are all almost completely resolved out with the EVN. However, the $\alpha_{1.4}^{8.4}$ spectral indices (Table 1) determined by Lal & Ho [11] are markedly different, with opposite sign, all indicating inverted spectra ($\alpha_{1.4}^{8.4} > 0.38$). Higher flux densities at 8.4 GHz, as seen in Figure 2, could in principle be caused by extreme variability, because the measurements at different frequencies were not made simultaneously. However, it is remarkable that all five sources show highly elevated flux densities at 8.4 GHz, rendering the variability explanation very unlikely, even though selection at higher frequencies such as 8.4 GHz would be biased to flat-spectrum, more variable sources.

Interestingly, among the lowest-power radio sources in the whole Type 2 quasar sample where our sources were selected from [11], the vast majority appear to have inverted spectra (see their Figure 6). This is even more puzzling in comparison with similar radio studies of Type 2 quasars [50,51] where these objects tend to have

steep ($\alpha < -0.5$) spectrum. The steep spectra indicate extended radio emission, explaining why we could not detect compact cores in four LLAGNs.

The compact VLBI component found in SDSS J1026–0042 appears to have a steep spectrum ($\alpha_{1.7}^5 = -1.73$). While this would not be unprecedented since steep-spectrum and even ultra-steep-spectrum ($\alpha < -1$) radio cores are often found in LLAGNs (e.g., [14,52–54]), we should treat this result with caution. The reason for the ill-determined core spectrum could be that the source is very weak, and model fitting to the EVN visibility data could be affected by phase-reference losses (e.g., [55]), especially at the higher frequency. This may have led to the underestimation of the flux density at 5 GHz, and consequently the core spectral index.

6. Conclusions

In this paper, we present 1.7- and 5-GHz EVN observations of five LLAGNs selected by their spectral (inverted-spectrum) and morphological (double-lobed symmetric) properties from [11]. Out of the five sources, only one (SDSS J1026–0042) was firmly detected with the EVN at both frequencies. It has a compact mas-scale VLBI core. The compact radio emission is a result of AGN activity. The other four sources (J0741+3020, J0956+5735, J1014+0244, and J1447+0211) are marginally detected at 1.7 GHz but not detected at 5 GHz with the EVN. It is consistent with dominantly extended, steep-spectrum radio emission in these objects.

With the help of VLASS data, we revised the radio spectral index for our five target sources. We found that they have flat or steep spectra between 1.4 and 2.7 GHz, contrary to the inverted spectra reported earlier [11]. The revised overall spectral properties are consistent with the outcome of the EVN observations, as the only flat-spectrum source (SDSS J1026–0042) contains a compact VLBI core. Based on our results, we suspect that spectral indices for at least some other inverted-spectrum LLAGNs found by Lal & Ho [11] may need to be revised. This could be done using new survey data becoming available such as those from the VLASS.

Because of the dubious sample selection, the applicability of our proposed method to find kpc-scale dual AGNs by targeting truly inverted-spectrum arcsec-scale symmetric double extragalactic radio sources with high-resolution VLBI imaging observations remains to be proven.

Author Contributions: Conceptualization and investigation, Z.P., R.D., and S.F.; Formal analysis, M.K. and S.F.; Writing—Original draft preparation, M.K. and S.F.; and writing—review and editing, Z.P. and R.D. All authors have read and agreed to the published version of the manuscript.

Funding: The research leading to these results has received funding from the European Commission Seventh Framework Programme (FP/2007–2013) under grant agreement No. 283393 (RadioNet3). This work is part of the project “Transient Astrophysical Objects” GINOP 2.3.2-15-2016-00033 of the National Research, Development and Innovation Office (NKFIH), Hungary, funded by the European Union.

Acknowledgments: The EVN is a joint facility of independent European, African, Asian, and North American radio astronomy institutes. Scientific results from data presented in this publication were derived from the project EP093. The National Radio Astronomy Observatory is a facility of the National Science Foundation operated under cooperative agreement by Associated Universities, Inc. This research has made use of the NASA/IPAC Extragalactic Database (NED), which is funded by the National Aeronautics and Space Administration and operated by the California Institute of Technology. Funding for the SDSS and SDSS-II has been provided by the Alfred P. Sloan Foundation, the Participating Institutions, the National Science Foundation, the U.S. Department of Energy, the National Aeronautics and Space Administration, the Japanese Monbukagakusho, the Max Planck Society, and the Higher Education Funding Council for England. The SDSS Web Site is <http://www.sdss.org/>. The SDSS is managed by the Astrophysical Research Consortium for the Participating Institutions. The Participating Institutions are the American Museum of Natural History, Astrophysical Institute Potsdam, University of Basel, University of Cambridge, Case Western Reserve University, University of Chicago, Drexel University, Fermilab, the Institute for Advanced Study, the Japan Participation Group, Johns Hopkins University, the Joint Institute for Nuclear Astrophysics, the Kavli Institute for Particle Astrophysics and Cosmology, the Korean Scientist Group, the Chinese Academy of Sciences (LAMOST), Los Alamos National Laboratory, the Max-Planck-Institute for Astronomy (MPIA), the Max-Planck-Institute for Astrophysics (MPA), New Mexico State University, Ohio State University, University of Pittsburgh, University of Portsmouth, Princeton University, the United States Naval Observatory, and the University of Washington. This work presents results from the European Space Agency (ESA) space mission *Gaia*. *Gaia* data are being processed by the *Gaia* Data Processing and Analysis Consortium (DPAC). Funding for the DPAC is provided by national institutions, in particular the institutions participating in the *Gaia*

MultiLateral Agreement (MLA). The *Gaia* mission website is <https://www.cosmos.esa.int/gaia>. The *Gaia* archive website is <https://archives.esac.esa.int/gaia>.

Conflicts of Interest: The authors declare no conflict of interest.

Abbreviations

The following abbreviations are used in this manuscript:

AGN	active galactic nucleus
AIPS	NRAO Astronomical Image Processing System
DR	data release
EVN	European VLBI Network
FIRST	Faint Images of the Radio Sky at Twenty Centimeters
FWHM	full width at half-maximum
HPBW	half-power beam width
JIVE	Joint Institute for VLBI European Research Infrastructure Consortium
LINER	low-ionization nuclear emission-line region
LLAGN	low-luminosity AGN
NRAO	U.S. National Radio Astronomy Observatory
NVSS	NRAO VLA Sky Survey
SDSS	Sloan Digital Sky Survey
SKA	Square Kilometre Array
SNR	signal-to-noise ratio
ULIRG	ultraluminous infrared galaxy
VLA	Karl G. Jansky Very Large Array
VLASS	Karl G. Jansky Very Large Array Sky Survey
VLBI	very long baseline interferometry

References

1. Ho, L.C.; Filippenko, A.V.; Sargent, W.L.W. A Search for “Dwarf” Seyfert Nuclei. III. Spectroscopic Parameters and Properties of the Host Galaxies. *Astrophys. J. Suppl. Ser.* **1997**, *112*, 315–390.
2. Falcke, H.; Nagar, N.M.; Wilson, A.S.; Ulvestad, J.S. Radio Sources in Low-Luminosity Active Galactic Nuclei. II. Very Long Baseline Interferometry Detections of Compact Radio Cores and Jets in a Sample of LINERs. *Astrophys. J.* **2000**, *542*, 197–200.
3. Nagar, N.M.; Falcke, H.; Wilson, A.S.; Ulvestad, J.S. Radio sources in low-luminosity active galactic nuclei. III. “AGNs” in a distance-limited sample of “LLAGNs”. *Astron. Astrophys.* **2002**, *392*, 53–82.
4. Falcke, H.; Biermann, P.L. The jet/disk symbiosis. III. What the radio cores in GRS 1915+105, NGC 4258, M 81 and Sgr A* tell us about accreting black holes. *Astron. Astrophys.* **1999**, *342*, 49–56.
5. Nagar, N.M.; Falcke, H.; Wilson, A.S. Radio sources in low-luminosity active galactic nuclei. IV. Radio luminosity function, importance of jet power, and radio properties of the complete Palomar sample. *Astron. Astrophys.* **2005**, *435*, 521–543.
6. Herrera Ruiz, N.; Middelberg, E.; Norris, R.P.; Maini, A. Unveiling the origin of the radio emission in radio-quiet quasars. *Astron. Astrophys.* **2016**, *589*, L2.
7. Kewley, L.J.; Heisler, C.A.; Dopita, M.A.; Sutherland, R.; Norris, R.P.; Reynolds, J.; Lumsden, S. Compact Radio Emission from Warm Infrared Galaxies. *Astrophys. J.* **2000**, *530*, 704–718.
8. Narayan, R.; Mahadevan, R.; Grindlay, J.E.; Popham, R.G.; Gammie, C. Advection-dominated accretion model of Sagittarius A*: Evidence for a black hole at the Galactic center. *Astron. J.* **1998**, *492*, 554–568.
9. Panessa, F.; Baldi, R.D.; Laor, A.; Padovani, P.; Behar, E.; McHardy, I. The origin of radio emission from radio-quiet active galactic nuclei. *Nat. Astron.* **2019**, *3*, 387–396.

10. Ulvestad, J.S.; Ho, L.C. The Origin of Radio Emission in Low-Luminosity Active Galactic Nuclei: Jets, Accretion Flows, or Both? *Astrophys. J.* **2001**, *562*, L133–L136.
11. Lal, D.V.; Ho, L.C. The Radio Properties of Type 2 Quasars. *Astron. J.* **2010**, *139*, 1089–1105.
12. Condon, J.J.; Huang, Z.-P.; Yin, Q. F.; Thuan, T.X. Compact Starbursts in Ultraluminous Infrared Galaxies. *Astron. J.* **1991**, *378*, 65–76.
13. Laor, A.; Baldi, R.D.; Behar, E. What drives the radio slopes in radio-quiet quasars? *Mon. Not. R. Astron. Soc.* **2019**, *482*, 5513–5523.
14. Fu, H.; Wrobel, J.M.; Myers, A.D.; Djorgovski, S.G.; Yan, L. Binary Active Galactic Nuclei in Stripe 82: Constraints on Synchronized Black Hole Accretion in Major Mergers. *Astrophys. J. Lett.* **2015**, *815*, L6.
15. Lacy, M.; Baum, S.A.; Chandler, C.J.; Chatterjee, S.; Clarke, T.E.; Deustua, S.; English, J.; Farnes, J.; Gaensler, B.M.; Gugliucci, N.; et al. The Karl G. Jansky Very Large Array Sky Survey (VLASS). Science Case and Survey Design. *Publ. Astron. Soc. Pac.* **2020**, *132*, 035001.
16. An, T.; Mohan, P.; Frey, S. VLBI studies of DAGN and SMBHB hosting galaxies. *Radio Sci.* **2018**, *53*, 1211–1217.
17. De Rosa, A.; Vignali, C.; Bogdanović, T.; Capelo, P.R.; Charisi, M.; Dotti, M.; Husemann, B.; Lusso, E.; Mayer, L.; Paragi, Z.; Runnoe, J.; et al. The Quest for Multiple Supermassive Black Holes: A Multi-Messenger View. *New Astron. Rev.* **2019**, *89*, 101525.
18. Bondi, M.; Pérez-Torres, M.-A. VLBI Detection of an Active Galactic Nucleus Pair in the Binary Black Hole Candidate SDSS J1536+0441. *Astrophys. J.* **2010**, *714*, L271–L274.
19. Laor, A.; Behar, E. On the origin of radio emission in radio-quiet quasars. *Mon. Not. R. Astron. Soc.* **2008**, *390*, 847–862.
20. Deane, R.; Paragi, Z.; Jarvis, M.; Coriat, M.; Bernardi, G.; Frey, S.; Heywood, I.; Kloeckner, H.R. Multiple supermassive black hole systems: SKA's future leading role. In Proceedings of Advancing Astrophysics with the Square Kilometre Array, Proceedings of Science, 2015; Volume AASKA14, 9–13 June, 2014. Giardini Naxos, Italy p. 151.
21. Ellison, S.L.; Secrest, N.J.; Mendel, J.T.; Satyapal, S.; Simard, L. Discovery of a dual active galactic nucleus with ~ 8 kpc separation. *Mon. Not. R. Astron. Soc.* **2017**, *470*, L49–L53.
22. Wright, E.L. A Cosmology Calculator for the World Wide Web. *Publ. Astron. Soc. Pac.* **2006**, *118*, 1711–1715.
23. Zakamska, N.L.; Strauss, M.A.; Krolik, J.H.; Collinge, M.J.; Hall, P.B.; Hao, L.; Heckman, T.M.; Ivezić, Ž.; Richards, G.T.; Schlegel, D.J.; et al. Candidate Type II Quasars from the Sloan Digital Sky Survey. I. Selection and Optical Properties of a Sample at $0.3 < z < 0.83$. *Astron. J.* **2003**, *126*, 2125–2144.
24. Bellocchi, E.; Villar Martín, M.; Cabrera-Lavers, A.; Emons, B. QSO2 outflow characterization using data obtained with OSIRIS at the Gran Telescopio Canarias. *Astron. Astrophys.* **2019**, *626*, A89.
25. Villar-Martín, M.; Cabrera Lavers, A.; Bessiere, P.; Tadhunter, C.; Rose, M.; de Breuck, C. Mergers and interactions in Sloan Digital Sky Survey type 2 quasars at $z \sim 0.3 - 0.4$. SDSS J143027.66–005614.8: A case study. *Mon. Not. R. Astron. Soc.* **2012**, *423*, 80–103.
26. Urbano-Mayorgas, J.J.; Villar Martín, M.; Buitrago, F.; Piqueras López, J.; Rodríguez del Pino, B.; Koekemoer, A.M.; Huertas-Company, M.; Domínguez-Tenreiro, R.; Carrera, F.J.; Tadhunter, C. The host galaxies of luminous type 2 AGNs at $z \sim 0.3 - 0.4$. *Mon. Not. R. Astron. Soc.* **2019**, *483*, 1829–1849.
27. Aguado, D.S.; Ahumada, R.; Almeida, A.; Anderson, S.F.; Andrews, B.H.; Anguiano, B.; Ortiz, E.A.; Salamanca, A.A.; Argudo-Fernandez, M.; Aubert, M.; et al. The Fifteenth Data Release of the Sloan Digital Sky Surveys: First Release of MaNGA-derived Quantities, Data Visualization Tools, and Stellar Library. *Astrophys. J. Suppl. Ser.* **2019**, *240*, 23.
28. Gaia Collaboration; Prusti, T.; de Bruijne, J.H.J.; Brown, A.G.A.; Vallenari, A.; Babusiaux, C.; Bailer-Jones, C.A.L.; Bastian, U.; Biermann, M.; Evans, D.W.; et al. The Gaia mission. *Astron. Astrophys.* **2016**, *595*, A1.
29. Gaia Collaboration; Brown, A.G.A.; Vallenari, A.; Prusti, T.; de Bruijne, J.H.J.; Babusiaux, C.; Bailer-Jones, C.A.L.; Biermann, M.; Evans, D.W.; Eyer, L.; et al. Gaia Data Release 2. Summary of the contents and survey properties. *Astron. Astrophys.* **2018**, *616*, A1.
30. Beasley, A.J.; Conway, J.E. VLBI Phase-Referencing. In *Very Long Baseline Interferometry and the VLBA*; ASP Conference Series 82; Zensus, J.A., Diamond, P.J., Napier, P.J., Eds.; Astronomical Society of the Pacific: San Francisco, CA, USA, 1995; pp. 327–343., Chapter 17.

31. Becker, R.H.; White, R.L.; Helfand, D.J. The FIRST Survey: Faint Images of the Radio Sky at Twenty Centimeters. *Astron. J.* **1995**, *450*, 559–577.
32. Condon, J.J.; Cotton, W.D.; Greisen, E.W.; Yin, Q.F.; Perley, R.A.; Taylor, G.B.; Broderick, J.J. The NRAO VLA Sky Survey. *Astron. J.* **1998**, *115*, 1693–1716.
33. Villarreal Hernández, A.C.; Andernach, H. A Search for Extended Radio Sources in 1.3 sr of the VLA Sky Survey (VLASS). *arXiv* **2018**, arXiv:1808.07178.
34. Diamond, P.J. VLBI Data Reduction in Practice. In *Very Long Baseline Interferometry and the VLBA*; ASP Conference Series 82; Zensus, J.A., Diamond, P.J., Napier, P.J., Eds.; Astronomical Society of the Pacific: San Francisco, CA, USA, 1995; pp. 327–343., Chapter 12.
35. Shepherd, M.C.; Pearson, T.J.; Taylor, G.B. DIFMAP: An interactive program for synthesis imaging. *Bull. Am. Astron. Soc.* **1994**, *26*, 987–989.
36. Lacy, M.; Myers, S.; Kimball, A.; Schinzel, F.; Chandler, C.; Sjouwerman, L.; Marvil, J.; Masters, J.; Medlin, D.; Vargas, A.; et al. Pilot and Epoch 1 Quick Look Data Release. VLASS Project Memo #13. 2019. Available online: https://safe.nrao.edu/wiki/pub/JVLA/VLASS/VLASS_Memo_013_Epoch_1_Quicklook_Data_Release.pdf (accessed on 27 February 2020).
37. Kovalev, Y.Y.; Kellermann, K.I.; Lister, M.L.; Homan, D.C.; Vermeulen, R.C.; Cohen, M.H.; Ros, E.; Kadler, M.; Lobanov, A.P.; Zensus, J.A.; et al. Sub-Milliarcsecond Imaging of Quasars and Active Galactic Nuclei. IV. Fine-Scale Structure. *Astron. J.* **2005**, *130*, 2473–2505.
38. Fomalont, E.B. Image Analysis. In *Synthesis Imaging in Radio Astronomy II*; ASP Conference Series 180; Taylor G.B., Carilli C.L., Perley R.A., Eds.; Astronomical Society of the Pacific: San Francisco, CA, USA, 1999; pp. 301–319.
39. Plavin, A.V.; Kovalev, Y.Y.; Petrov, L.Y. Dissecting the AGN Disk-Jet System with Joint VLBI-Gaia Analysis. *Astron. J.* **2019**, *871*, 143.
40. Kovalev, Y.Y.; Petrov, L.; Plavin, A.V. VLBI-Gaia offsets favor parsec-scale jet direction in active galactic nuclei. *Astron. Astrophys.* **2017**, *598*, L1.
41. Petrov, L.; Kovalev, Y.Y. Observational consequences of optical band milliarcsec-scale structure in active galactic nuclei discovered by Gaia. *Mon. Not. R. Astron. Soc.* **2017**, *471*, 3775–3787.
42. Condon, J.J.; Condon, M.A.; Gisler, G.; Puschell, J.J. Strong radio sources in bright spiral galaxies. II. Rapid star formation and galaxy-galaxy interactions. *Astron. J.* **1982**, *252*, 102–124.
43. Mannucci, F.; Maiolino, R.; Cresci, G.; Della Valle, M.; Vanzi, L.; Ghinassi, F.; Ivanov, V.D.; Nagar, N.M.; Alonso-Herrero, A. The infrared supernova rate in starburst galaxies. *Astron. Astrophys.* **2003**, *401*, 519–530.
44. Bondi, M.; Pérez-Torres, M.A.; Herrero-Illana, R.; Alberdi, A. The nuclear starburst in Arp 299-A: From the 5.0 GHz VLBI radio light-curves to its core-collapse supernova rate. *Astron. Astrophys.* **2012**, *539*, A134.
45. Zakamska, N.L.; Lampayan, K.; Petric, A.; Dicken, D.; Greene, J.E.; Heckman, T.M.; Hickox, R.C.; Ho, L.C.; Krolik, J.H.; Nesvadba, N.P.H.; et al. Star formation in quasar hosts and the origin of radio emission in radio-quiet quasars. *Mon. Not. R. Astron. Soc.* **2016**, *455*, 4191–4211.
46. Maini, A.; Prandoni, I.; Norris, R.P.; Giovannini, G.; Spitler, L.R. Compact radio cores in radio-quiet active galactic nuclei. *Astron. Astrophys.* **2016**, *589*, L3.
47. Strauss, M.A.; Weinberg, D.H.; Lupton, R.H., et al. Spectroscopic Target Selection in the Sloan Digital Sky Survey: The Main Galaxy Sample. *Astron. J.* **2002**, *124*, 1810–1824.
48. Orosz, G.; Frey, S. Optical-radio positional offsets for active galactic nuclei. *Astron. Astrophys.* **2013**, *553*, A13.
49. Skipper, C.J.; Browne, I.W.A. Spatially offset AGN candidates in the CLASS survey. *Mon. Not. R. Astron. Soc.* **2018**, *475*, 5179–5193.
50. Martínez-Sansigre, A.; Rawlings, S.; Garn, T.; Green, D.A.; Alexander, P.; Klöckner, H.-R.; Riley, J.M. A population of high-redshift type 2 quasars—II. Radio properties. *Mon. Not. R. Astron. Soc.* **2006**, *373*, L80–L84.
51. Zakamska, N.L.; Strauss, M.A.; Heckman, T.M.; Ivezić, Ž.; Krolik, J.H. Candidate Type II Quasars from the Sloan Digital Sky Survey. II. From Radio to X-Rays. *Astron. J.* **2004**, *128*, 1002–1016.
52. Argo, M.K.; Paragi, Z.; Röttgering, H.; Klöckner, H.-R.; Miley, G.; Mahmud, M. Probing the nature of compact ultrasteepest spectrum radio sources with the e-EVN and e-MERLIN. *Mon. Not. R. Astron. Soc.* **2013**, *431*, L58–L62.

53. Kharb, P.; Subramanian, S.; Vaddi, S.; Das, M.; Paragi, Z. Double-peaked Emission Lines Due to a Radio Outflow in KISSR 1219. *Astrophys. J.* **2017**, *846*, 12.
54. Kharb, P.; Lena, D.; Paragi, Z.; Subramanian, S.; Vaddi, S.; Das, M.; Khatun, R. The Intriguing Parsec-scale Radio Structure in the “Offset AGN” KISSR 102. *Astrophys. J.* **2020**, *890*, 40.
55. Martí-Vidal, I.; Ros, E.; Pérez-Torres, M.A.; Guirado, J.C.; Jiménez-Monferrer, S.; Marcaide, J.M. Coherence loss in phase-referenced VLBI observations. *Astron. Astrophys.* **2010**, *515*, A53.

© 2020 by the authors. Licensee MDPI, Basel, Switzerland. This article is an open access article distributed under the terms and conditions of the Creative Commons Attribution (CC BY) license (<http://creativecommons.org/licenses/by/4.0/>).

